Characterization of Single Nucleotide Variants of *OPN3* Gene in Melanocytic Nevi and Melanoma

Wei Zhang[1,4], Jianglong Feng[2,4], Wen Zeng[1,4], Zhixu Zhou[3], Yu Wang[1] and Hongguang Lu[1]

In this study, we examined single nucleotide variants (SNVs) of the *OPN3* gene in malignant melanoma and melanocytic nevi. A total of 20 variants of SNVs were detected. Of these variants, five nonsynonymous mutations of *OPN3* were identified, including c.T152C, c.T401C, c.G547A, c.G768A, and c.G992A. Three prediction tools, MutationTaster2, Polymorphism Phenotyping version 2, and PROVEAN (Protein Variation Effect Analyzer), which predict possible impact of an amino acid substitution, suggested that the mutations could be deleterious. Nine SNVs occurred in 3′ untranslated regions, whereas two were observed in 5′ untranslated regions. In all cases, four intronic variants were identified. In addition, we identified nine 3′ untranslated region SNVs in *OPN3*; one of them (OPN3[NM_014322:c.*83C>T]) is predicted to disrupt a conserved microRNA (has-miR-376c-3p) target site, located in position 86−93 of *OPN3* 3′ untranslated region. Our findings suggest that there is a strong possibility that *OPN3* SNVs play a role in the pathogenesis of melanocytic tumors via prediction of functional phenotype.

JID Innovations (2021);**1:**100006 doi:10.1016/j.xjidi.2021.100006

INTRODUCTION

First described by Blackshaw and Snyder (1999), OPN3 was identified as a mammalian extraocular opsin. It is highly conserved throughout vertebrates as an ancestral type of opsin (Fischer et al., 2013). On the genomic level, *OPN3* is composed of four exons on human chromosome 1q43, encompassing two flanking genes, *CHML* and *KMO*. *CHML*, a single exon gene, resides in intron 1 of *OPN3*, whereas *KMO* and *OPN3* overlap with their 3′-untranslated regions (UTRs), which are transcribed in opposite directions (Halford et al., 2001). Recently, we and others have found that OPN3 is highly expressed in human epidermal melanocytes compared with other opsins (Ozdeslik et al., 2019; Regazzetti et al., 2018; Wang et al., 2020). These studies further demonstrated that OPN3 mediates nonvisual functions such as melanogenesis and apoptosis in melanocytes. In addition, previous studies of the relationship between *OPN3* and human diseases showed that *OPN3* is identified as an asthma susceptibility gene (White et al., 2008). Miyanaga et al. (2020) recently found that *OPN3* is upregulated in pulmonary carcinoid tumors that developed postsurgical metastasis. With The Cancer Genome Atlas data analysis, we also observed that *OPN3* expression is upregulated in human melanoma compared with normal skin (NS) (Figure 1). Although its role in benign and malignant melanocytic lesions remains uncharacterized, based on these studies, it is likely that OPN3 modulates proliferation, pigmentation, and apoptosis of malignant melanocytes in tumor initiation and progression.

RESULTS

Here, we performed single nucleotide variant (SNV) analysis of *OPN3* in 68 malignant melanoma (MM), 166 melanocytic nevi (MNs), and 42 NS tissues from a Chinese population (Table 1). This study of formalin-fixed, paraffin-embedded tissues was approved by the ethics committee of Affiliated Hospital of Guizhou Medical University (Guiyang, China). Five nonsynonymous mutations were identified in the melanocytic lesions, including c.T152C, c.T401C, c.G547A, c.G768A, and c.G992A (Table 2). The c.T152C mutation was detected in one case of acral lentiginous melanoma. For the c.T401C mutation, MM mutations were much more common than MN and NS mutations, which were not associated with sex, age, localization, or histological subtype of samples. In addition, no significant differences were seen for SNVs in *OPN3* in MM, MN, and NS (Table 2). In the c.G768A mutation of MM and MN, all five MM lesions displayed acral lentiginous melanoma. Of them, three MNs were found to be junctional nevi, and two were compound nevi. Overall, 3 of 68 MMs (4.41%) and 14 of 166 MNs (8.43%) revealed simultaneous *OPN3* and *BRAF V600E* mutations. In 2 of 40 acral lentiginous melanoma cases (5%) with hotspot mutant *BRAF V600E*, the c.G768A mutation in *OPN3* was also identified. In MM, the remaining one case with two mutations was metastatic melanoma (Table 3).

[1]*Department of Dermatology, Affiliated Hospital of Guizhou Medical University, Guiyang, China;* [2]*Department of Pathology, Affiliated Hospital of Guizhou Medical University, Guiyang, China; and* [3]*School of Pharmaceutical Sciences, Guizhou University, Guiyang, China*

[4]*These authors contributed equally to this work.*

Correspondence: Hongguang Lu, Department of Dermatology, Affiliated Hospital of Guizhou Medical University. No. 28 Guiyi Road, Guiyang 550001, China. E-mail: hongguanglu@hotmail.com

Abbreviations: miRNA, microRNA; MM, malignant melanoma; MN, melanocytic nevus; NS, normal skin; SNV, single nucleotide variant; UTR, untranslated region

Received 3 December 2020; revised 21 January 2021; accepted 22 January 2021; accepted manuscript published online 26 February 2021

Cite this article as: JID Innovations 2021;1:100006

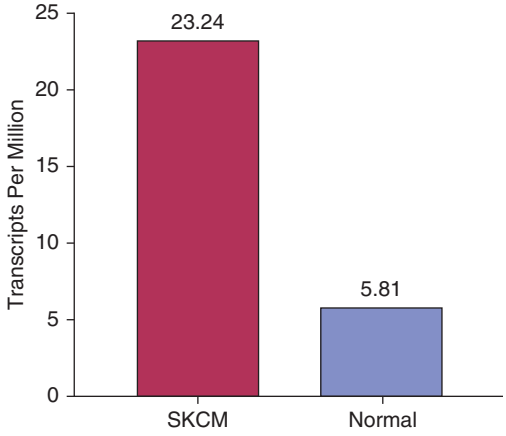

Figure 1. *OPN3* expression profile between SKCM (n = 461) and paired normal tissues (n = 558) based on TCGA data analysis. The height of each bar represents the median expression. The expression of *OPN3* in SKCM is higher than that in normal tissues. SKCM, skin cutaneous melanoma; TCGA, The Cancer Genome Atlas.

We predicted the functional consequences of amino acid substitutions via three prediction tools (Polymorphism Phenotyping version 2, PROVEAN [Protein Variation Effect Analyzer], MutationTaster2) to evaluate the pathogenic potential of these nonsynonymous mutations (Table 4) (Schwarz et al., 2014). The prediction results of the c.G768A variant by the three tools was the most consistent, suggesting that it has deleterious effects. The results of two prediction tools showed that the c.T152C variant was also probably damaging. Other mutations were predicted to be deleterious by one of the three prediction tools. Moreover, mutant protein three-dimensional models were generated via the remote homology detection method of Phyre2 (Kelley et al., 2015) (Figure 2).

In addition, nine SNVs in the 3′-UTR and two SNVs in the 5′-UTR of *OPN3* were found in all MN and MM samples, including four novel SNVs of 3′-UTR: *KMO*(c.*1932G>C), *OPN3*(c.*343C>G); *KMO*(c.*1955_*1956insA), *OPN3*(-c.*319_*320insT); *KMO*(c.*2146C>T), *OPN3*(c.*129G>A); and *KMO*(c.*2192G>A), *OPN3*(c.*83C>T) (Table 2). Two SNVs (*OPN3*[c.-80A>G] and *OPN3*[c.-102T>C]) in the 5′-UTR occurred in the same cases. Only two SNVs in the 3′-UTR (*OPN3*[c.*319_*320insT], rs3765809) were detected in the NS control group. The homozygote (*TT*) variant of rs3765809 had significant differences between the MN and NS groups ($P < 0.05$). Furthermore, we predicted the effects of SNVs in the 3′-UTR via miRDB and TargetscanHuman7.2 (Peng et al., 2020), which predicted microRNA (miRNA) targets in mammals. In 3′-UTR variants, as biological targets of miRNAs, seven miRNAs (has-miR-1272, has-miR-1267, has-miR-376c-3p, has-miR-6507-3p, has-miR-10399-5p, has-miR-137-5p, and has-miR-376c-3p) were predicted, one (has-miR-376c-3p) of them with a conserved 8mer (monomeric unit) site. This 3′-UTR SNV was detected in one intradermal nevus. In addition, four intronic SNVs were detected in all samples, including rs45572340, *OPN3* 241767624_53 T>G, rs140858921, and rs632966 (Table 2).

Table 1. Participants' Characteristics of the Study from Chinese Patients with MN, MM, and NS

	MN		MM		NS
Subject	**Total (n)**	***BRAF*^{V600E} (n)**	**Total (n)**	***BRAF*^{V600E} (n)**	**Total (n)**
Number	166	81	68	7	42
Sex					
Male	67	27	29	4	18
Female	99	54	39	3	26
Age, median (IQR)	30.0 (18.0–47.0)	33.00 (23.00–47.00)	65.0 (53.0–72.0)	42.0 (39.0–57.0)	44.0 (35.0–60.0)
Anatomical site					
Head	16	10	1	0	3
Face	78	54	4	0	13
Neck	4	3	0	0	4
Trunk	15	9	3	2	11
Limbs	24	1	6	2	6
Hand	9	0	10	1	3
Foot	20	4	39	2	2
Brain	—	—	2	0	#
Lymph node	—	—	3	0	#
Subtype					
Junctional nevus	28	3	—	—	—
Compound nevus	52	29	—	—	—
Intradermal nevus	53	49	—	—	—
Blue nevus	33	0	—	—	—
Superficial spreading melanoma	—	—	10	1	—
Nodular melanoma	—	—	7	2	—
Lentigo maligna melanoma	—	—	4	0	—
Acral lentiginous melanoma	—	—	40	2	—

Abbreviations: IQR, interquartile range; MM, malignant melanoma; MN, melanocytic nevus; NS, normal skin.
BRAF^{V600E} status was previously assessed by direct sequencing (Sanger) in all cases.

Table 2. Analysis of *OPN3* SNVs in MM, MN, and NS Groups

OPN3 SNVs	MM (n = 68), %	MN (n = 166), %	NS (n = 42), %	*P*-Value
Exon				
Exon 1 c.T152C A>G				
AG	1.47 (1/68)	0	0	0.2106
AA	97.06 (66/68)	100 (166/166)	100 (42/42)	
NA	1.47 (1/68)	0	0	
Exon 2 c.T401C A>G				
AG	4.41 (3/68)	1.20 (2/166)	2.38 (1/42)	0.1122
AA	92.65 (63/68)	98.80 (164/166)	97.6 (41/42)	
GG	1.47 (1/68)	0	0	
NA	1.47 (1/68)	0	0	
Exon 2 c.G547A C>T				
CT	10.29 (7/68)	9.04 (15/166)	14.28 (6/42)	0.6810
CC	93.93 (60/66)	90.36 (150/166)	85.71 (36/42)	
TT	0	0.60 (1/166)	0	
NA	1.47 (1/68)	0	0	
Exon 3 c.G768A C>T				
CT	7.35 (5/68)	3.01 (5/166)	9.52 (4/42)	0.1440
CC	92.66 (63/68)	95.78 (159/166)	90.48 (38/42)	
NA	0	1.20 (2/166)	0	
Exon 4 c.G992A C>T				
CT	0	1.81 (3/166)	2.38 (1/42)	0.4948
CC	98.53 (67/68)	97.60 (162/166)	97.6 (41/42)	
NA	1.47 (1/68)	0.60 (1/166)	0	
3′-UTR				
KMO(c.*1253G>A), *OPN3*(c.*1022C>T) rs371271799				
GA	1.47 (1/68)	0	0	0.2663
GG	66.18 (45/68)	47.59 (79/166)	100 (42/42)	
NA	32.35 (22/68)	52.41 (87/166)	0	
KMO(c.*1498A>G), *OPN3*(c.*777T>C) rs144936606				
AG	1.47 (1/68)	0.60 (1/166)	0	0.6418
AA	97.06 (66/68)	99.40 (165/166)	100 (42/42)	
NA	1.47 (1/68)	0	0	
KMO(c.*1932G>C), *OPN3*(c.*343C>G)				
GC	1.47 (1/68)	0	0	0.2086
GG	94.12 (64/68)	96.99 (161/166)	100 (42/42)	
NA	4.41 (3/68)	3.01 (5/166)	0	
KMO(c.*1955_*1956insA),*OPN3*(c.*319_*320insT)				
A/ins_A	38.24 (26/68)	37.35 (62/166)	28.57 (12/42)	0.5028
A/A	60.29 (41/68)	62.05 (103/166)	71.43 (30/42)	
NA	1.47 (1/68)	0.60 (1/166)	0	
KMO(c.*2094G>T), *OPN3*(c.*181C>A) rs3765809				
GT	13.24 (9/68)	15.06 (25/166)	19.05 (8/42)	0.7272
TT	0	0	4.76 (2/42)	0.0404[2]
GG	85.29 (58/68)	84.34 (140/166)	76.19 (32/42)	
NA	1.47 (1/68)	0.60 (1/166)	0	
KMO(c.*2146C>T), *OPN3*(c.*129G>A)				
CT	0	1.20 (2/166)	0	0.5140
CC	98.53 (67/68)	98.19 (163/166)	100 (42/42)	
NA	1.47 (1/68)	0.60 (1/166)	0	
KMO(c.*2192G>A), *OPN3*(c.*83C>T)				
GA	0	0.60 (1/166)	0	0.7171
GG	100 (68/68)	99.40 (165/166)	100 (42/42)	
NA	0	0	0	
KMO(c.*2258G>A), *OPN3*(c.*17C>T) rs199779503				
GA	1.47 (1/68)	0	0	0.2122
GG	97.06 (66/68)	99.40 (165/166)	100 (42/42)	
NA	1.47 (1/68)	0.60 (1/166)	0	

(*continued*)

Table 2. Continued

OPN3 SNVs	MM (n = 68), %	MN (n = 166), %	NS (n = 42), %	*P*-Value
KMO(c.*2267C>G), *OPN3*(c.*8G>C) rs201495076				
CG	1.47 (1/68)	1.20 (2/166)	0	0.7469
CC	97.06 (66/68)	98.19 (163/166)	100 (42/42)	
NA	1.47 (1/68)	0.60 (1/166)	0	
5′-UTR				
OPN3(c.-80A>G) rs7513575				
TC	1.47 (1/68)	0.60 (1/166)	0	—
CC	1.47 (1/68)	0	100 (42/42)	
NA	97.06 (66/68)	99.40 (165/166)	0	
OPN3(c.-102T>C) rs7513451				
AG	1.47 (1/68)	0.60 (1/166)	0	—
GG	1.47 (1/68)	0	100 (42/42)	
NA	97.06 (66/68)	99.40 (165/166)	0	
Intron				
rs45572340 T>C				
TC	8.82 (6/68)	9.04 (15/166)	11.90 (5/42)	0.8494
CC	2.94 (2/68)	0.60 (1/166)	0	0.2244
TT	85.29 (58/68)	89.76 (149/166)	88.10 (37/42)	
NA	2.94 (2/68)	0.60 (1/166)	0	
OPN3 241767624_53 T>G				
TG	1.47 (1/68)	0	0	0.2051
TT	92.65 (63/68)	96.39 (160/166)	0	
NA	5.8 (4/68)	3.61 (6/166)	100 (42/42)	
rs140858921 A>G				
AG	4.41 (3/68)	4.22 (7/166)	0	0.3931
GG	0	0.60 (1/166)	0	0.7185
AA	89.71 (61/68)	91.57 (152/166)	100 (42/42)	
NA	5.8 (4/68)	3.61 (6/166)	0	
rs632966 G>A				
GA	30.88 (21/68)	33.73 (56/166)	21.43 (9/42)	0.3058
AA	64.71 (44/68)	62.05 (103/166)	76.19 (32/42)	0.2297
GG	4.41 (3/68)	4.22 (7/166)	2.38 (1/42)	
NA	0	0	0	

Abbreviations: MM, malignant melanoma; MN, melanocytic nevus; NA, not applicable; NS, normal skin; SNV, single nucleotide variant; UTR, untranslated region.
[1]Two groups were compared by Fisher's exact test.
[2]$P < 0.05$.

DISCUSSION

In this study, we comprehensively identified *OPN3* genetic variants in patients with MM or MN. Five nonsynonymous SNVs of *OPN3* were detected in our results, and predictions of functional phenotypes provided evidence that these SNVs altered OPN3 conservation, especially for c.G768A, suggesting that this missense variant is deleterious. Crystal structure of OPN3 has been not resolved; we constructed the

Table 3. *OPN3* Nonsynonymous SNVs in MM, MN, and NS

OPN3 Mutation	Base Substitution	Amino Acid Substitution	MM (n = 68)	MS (n = 166)	NS (n = 42)	Concomitant *BRAF V600E* Mutation	
						MM	MN
Exon 1	c.T152C A>G	Ile>Thr	1	0	0	0	—
Exon 2	c.T401C A>G	Val>Ala	4	2	1	0	2
Exon 2	c.G547A C>T	Val>Ile	7	15	6	1	9
Exon 3	c.G768A C>T	Met>Ile	5	5	4	2	1
Exon 4	c.G992A C>T	Cys>Tyr	0	3	1	—	2

Abbreviations: Ala, alanine; Cys, cysteine; Ile, isoleucine; Met, methionine; MM, malignant melanoma; MN, melanocytic nevus; NS, normal skin; SNV, single nucleotide variant; Thr, threonine; Val, valine.

Table 4. Prediction Evaluation for *OPN3* Nonsynonymous SNVs with Three Kinds of Bioinformatics Software (PolyPhen-2, PROVEAN, MutationTaster2)

			PolyPhen-2			PROVEAN		MutationTaster2		
OPN3 Mutation	Base Substitution	NCBI dbSNP Reference ID	HumDiv (0–1)	HumVar (0–1)	Prediction	Score (−14 to 14)	Prediction (Cutoff = −2.5)	PhyloP (−14 to 6)	PhastCons (0–1)	Prediction
Exon 1	c.T152C A>G	rs201734451	0.180	0.025	Benign	−7.63	Deleterious	1.404	0.991	Disease causing
Exon 2	c.T401C A>G	rs117720055	0.116	0.057	Benign	−9.15	Deleterious	0.693	0.627	Polymorphism
Exon 2	c.G547A C>T	rs2273712	0.001	0.002	Benign	−8.83	Deleterious	−0.604	0	Polymorphism
Exon 3	c.G768A C>T	rs78202695	0.985	0.977	Probably damaging	−4.76	Deleterious	5.232	1	Disease causing
Exon 4	c.G992A C>T	rs180909883	0.146	0.024	Benign	−2.10	Neutral	1.4	1	Disease causing

Abbreviations: dbSNP, SNP database; Div, division; Hum, human; ID, identification; NCBI, National Center for Biotechnology Information; PolyPhen-2, Polymorphism Phenotyping version 2; PROVEAN, Protein Variation Effect Analyzer; SNV, single nucleotide variant; Var, variant.

mutant three-dimensional structures of OPN3 by homology modeling based on OPN2. Although we could not demonstrate a significant statistical difference between MM and MN in *OPN3* SNVs, which may be due to the small sample size and therefore lack of statistical power, some implications can be suggested. OPN3 is a cell surface receptor of the G-protein coupled receptor family that plays a vital role in the regulation of proliferation, migration, and survival (Bar-Shavit et al., 2016). In addition, OPN3 expression influences melanocyte apoptosis (Wang et al., 2020). Therefore, c.G768A or other nonsynonymous SNVs could alter OPN3 protein structure and function and have an impact on melanocytic proliferation and apoptosis in MM and MN. *BRAF* mutations are low frequency in nature (about 15%) (Nakamura and Fujisawa, 2018). In all 40 samples of acral lentiginous melanoma, only two cases showed the *BRAF V600E* mutation. Both of them also contained the c.G768A variant in *OPN3*. This suggested that the products of multiple gene mutations may affect melanocytic proliferation and tumor formation. In addition, the 3′-UTR SNV (OPN3[NM_014322:c.*83C>T]) is predicted to disrupt a conserved miRNA (has-miR-376c-3p) target site, located in position 86–93 of *OPN3* 3′-UTR. It is possible that this UTR SNV might influence RNA stability or posttranscriptional regulation of *OPN3* (Mayr, 2017), which may restrain melanocytic proliferation and malignant transformation by downregulation of *OPN3* expression.

In this study, because we focused on overall *OPN3* SNVs, additional investigation will be necessary to further elucidate whether or not these variants affect the formation and growth of melanocytic lesions.

MATERIALS AND METHODS

Study population and data collection

All subjects with MMs and MNs were collected at Affiliated Hospital of Guizhou Medical University from January 2015 to December 2019 (Table 1). The control skin samples were obtained from normal adjacent nevi tissues. H&E-stained sections were reviewed by an experienced pathologist, and cases fulfilling criteria for the appropriate diagnoses (MM and MN) were selected for study. The study was approved by the Ethics Committees of our institution (Affiliated Hospital of Guizhou Medical University) and was performed according to the Declaration of Helsinki.

DNA extraction

DNA extraction from formalin-fixed, paraffin-embedded tissue was performed using an FFPE DNA Extraction Kit (AmoyDx, Xiamen, China), following the manufacturer's instructions. We measured the concentration of DNA using a Qubit 2.0 (Thermo Fisher Scientific, Waltham, MA) to ensure that adequate amounts of high-quality genomic DNA had been extracted.

Multiplex PCR and sequencing as described by Wei et al. (2020)

Library preparation was performed by two-step PCR. The first round PCR reaction was set up as follows: DNA (10 ng/μl) 2 μl; amplicon PCR forward primer mix (10 μM) 1 μl; amplicon PCR reverse primer mix (10 μM) 1 μl; and 2× PCR Ready Mix 15 μl (total 25 μl) (Kapa HiFi Ready Mix). The plate was sealed and PCR performed in a thermal instrument (T100TM, Bio-Rad, Hercules, CA) using the following program: one cycle of denaturing at 98 °C for 5 minutes, eight cycles of denaturing at 98 °C for 30 seconds, annealing at 50 °C for 30 seconds, elongation at 72 °C for 30 seconds, 25 cycles of denaturing at 98 °C for 30 seconds, annealing at 66 °C for 30 seconds, elongation at 72 °C for 30 seconds, and a final extension at 72 °C for 5 minutes with a final hold at 4 °C. The PCR products were checked using electrophoresis in 1 % (w/v) agarose gels in Tris, boric acid, and EDTA buffer stained with ethidium bromide and visualized under UV light. Then we used AMPure XP beads to purify the amplicon product. After that, the second round of PCR was performed. PCR reaction was set up as follows: DNA (10 ng/μl) 2 μl; universal P7 primer with barcode (10 μM) 1 μl; universal P5 primer (10 μM) 1 μl; and ×2 PCR Ready Mix 15 μl (total 30 μl) (Kapa HiFi Ready Mix). The plate was sealed, and PCR performed in a thermal instrument (T100TM, Bio-Rad) using the following program: one cycle of denaturing at 98 °C for 3 minutes, five cycles of denaturing at 94 °C for 30 seconds, annealing at 55 °C for 20 seconds, elongation at 72 °C for 30 seconds, and a final extension at 72 °C for 5 minutes. Then we used AMPure XP beads to purify the amplicon product. The libraries were then quantified and pooled. Paired-end sequencing of the library was performed on the HiSeq XTen sequencers (Illumina, San Diego, CA).

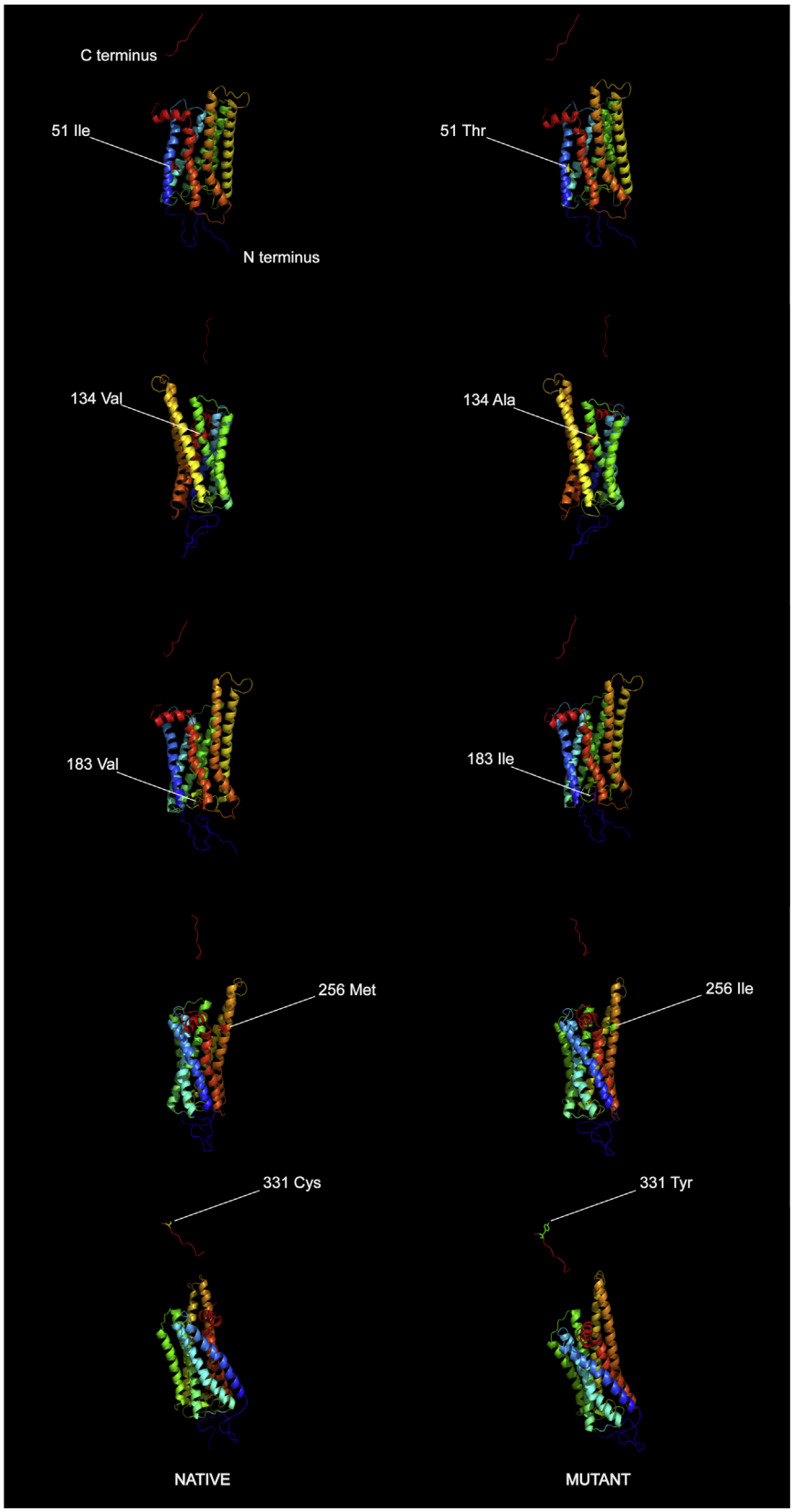

Figure 2. Mutant 3D models for all five nsSNVs in *OPN3* generated by Phyre2 server. 3D, three-dimensional; Ala, alanine; Cys, cysteine; Ile, isoleucine; Met, methionine; nsSNV, nonsynonymous single nucleotide variant; Thr, threonine; Tyr, tyrosine; Val, valine.

Data quality control and SNV calling as described by Wei et al. (2020)

Raw reads were filtered according to two steps: (i) removing adaptor sequence if reads contain by cutadapt (version 1.2.1) and (ii) removing low quality bases from reads 3′−5′ (Q < 20) by PRINSEQ-lite (version 0.20.3). The remaining clean data were mapped to the reference genome by BWA (version 0.7.13-r1126) with default parameters. SAMtools (version: 0.1.18) was used to calculate each genotype of target site. ANNOVAR (16 April 2018) was used to detect genetic variants.

Prediction of amino acid substitution

We evaluated the functional consequences of amino acid substitutions via three prediction tools, Polymorphism Phenotyping version 2 (http://genetics.bwh.harvard.edu/pph2/), PROVEAN (http://provean.jcvi.org/index.php), and MutationTaster2 (http://www.mutationtaster.org/), and compared predictions of the three tools on *OPN3* nonsynonymous SNVs. The web versions of the three prediction tools are used to predict the pathogenic potential of DNA sequence alterations. In addition, we built three-dimensional models of OPN3 to analyze the effect of SNVs on the protein sequence using SWISS-MODEL (https://swissmodel.expasy.org/). We also predicted the
effects of SNVs in the 3′-UTR via miRDB (http://mirdb.org/) and TargetscanHuman7.2 (http://www.targetscan.org/vert_72/), which predicted miRNA targets in mammals. Details about the methods and further statistics followed their websites and previous reports.

Statistical analyses

All data were entered into GraphPad Prism (version 8.0) for statistical analysis. Categorical data were analyzed using Fisher's exact test. A two-tailed $P < 0.05$ was considered statistically significant.

Data availability statement

No large datasets were generated or analyzed during this study. Minimal datasets necessary to interpret and/or replicate data in this paper are available on request to the corresponding author.

Ethics Statement

This study of formalin-fixed, paraffin-embedded tissues was approved by the ethics committee of Affiliated Hospital of Guizhou Medical University (Guiyang, China). Under Chinese law, written consent from the patients was not required because the material used had been collected for diagnostic and therapeutic purposes in the archives of the Institute for Pathology, Affiliated Hospital of Guizhou Medical University (Guiyang, China) and used for this study in pseudonymized form.

ORCIDs

Wei Zhang: http://orcid.org/0000-0003-1796-0182
Jianglong Feng: http://orcid.org/0000-0002-3667-415X
Wen Zeng: https://orcid.org/0000-0002-8251-4624
Zhixu Zhou: http://ocid.org/0000-0002-9633-9521
Yu Wang: http://orcid.org/0000-0002-8043-9165
Hongguang Lu: http://orcid.org/0000-0002-5002-4276

AUTHOR CONTRIBUTIONS

Conceptualization: HL, YW, WZh; Data Curation: JF, WZe; Formal Analysis: WZh, WZe, ZZ; Funding Acquisition: HL; Writing - Original Draft Preparation: WZh, HL; Writing - Review and Editing: HL

ACKNOWLEDGMENTS

This study was supported by the National Natural Science Foundation of China (81673069, 81972920). Under Chinese law, written consent from the patients was not required because the material used had been collected for diagnostic and therapeutic purposes in the archives of the Institute for Pathology, Affiliated Hospital of Guizhou Medical University (Guiyang, China) and used for this study in pseudonymized form. All authors contributed to results interpretations.

CONFLICT OF INTEREST

The authors state no conflict of interest.

REFERENCES

Bar-Shavit R, Maoz M, Kancharla A, Nag JK, Agranovich D, Grisaru-Granovsky S, et al. G protein-coupled receptors in cancer. Int J Mol Sci 2016;17:1320.

Blackshaw S, Snyder SH. Encephalopsin: a novel mammalian extraretinal opsin discretely localized in the brain. J Neurosci 1999;19:3681−90.

Fischer RM, Fontinha BM, Kirchmaier S, Steger J, Bloch S, Inoue D, et al. Co-expression of VAL- and TMT-opsins uncovers ancient photosensory interneurons and motorneurons in the vertebrate brain. PLoS Biol 2013;11:e1001585.

Halford S, Bellingham J, Ocaka L, Fox M, Johnson S, Foster RG, et al. Assignment of panopsin (OPN3) to human chromosome band 1q43 by in situ hybridization and somatic cell hybrids. Cytogenet Cell Genet 2001;95:234−5.

Kelley LA, Mezulis S, Yates CM, Wass MN, Sternberg MJE. The Phyre2 web portal for protein modeling, prediction and analysis. Nat Protoc 2015;10:845−58.

Mayr C. Regulation by 3′-untranslated regions. Annu Rev Genet 2017;51:171−94.

Miyanaga A, Masuda M, Motoi N, Tsuta K, Nakamura Y, Nishijima N, et al. Whole-exome and RNA sequencing of pulmonary carcinoid reveals chromosomal rearrangements associated with recurrence. Lung Cancer 2020;145:85−94.

Nakamura Y, Fujisawa Y. Diagnosis and management of acral lentiginous melanoma. Curr Treat Options Oncol 2018;19:42.

Ozdeslik RN, Olinski LE, Trieu MM, Oprian DD, Oancea E. Human nonvisual opsin 3 regulates pigmentation of epidermal melanocytes through functional interaction with melanocortin 1 receptor. Proc Natl Acad Sci USA 2019;116:11508−17.

Peng J, Liu F, Zheng H, Wu Q, Liu S. Long noncoding RNA ZFAS1 promotes tumorigenesis and metastasis in nasopharyngeal carcinoma by sponging miR-892b to up-regulate LPAR1 expression. J Cell Mol Med 2020;24:1437−50.

Regazzetti C, Sormani L, Debayle D, Bernerd F, Tulic MK, De Donatis GM, et al. Melanocytes sense blue light and regulate pigmentation through Opsin-3. J Invest Dermatol 2018;138:171−8.

Schwarz JM, Cooper DN, Schuelke M, Seelow D. MutationTaster2: mutation prediction for the deep-sequencing age. Nat Methods 2014;11:361−2.

Wang Y, Lan Y, Lu H. Opsin3 downregulation induces apoptosis of human epidermal melanocytes via mitochondrial pathway. Photochem Photobiol 2020;96:83−93.

Wei BL, Yin RX, Liu CX, Deng GX, Guan YZ, Zheng PF. The MC4R SNPs, their haplotypes and gene-environment interactions on the risk of obesity. Mol Med 2020;26:77.

White JH, Chiano M, Wigglesworth M, Geske R, Riley J, White N, et al. Identification of a novel asthma susceptibility gene on chromosome 1qter and its functional evaluation. Hum Mol Genet 2008;17:1890−903.